Proceedings of the 2015
IEEE Conference on Robotics and Biomimetics
Zhuhai, China, December 6-9, 2015

Detecting Optic Disk Based on Structured Learning

Zhun Fan[1], Yibiao Rong[2], Xinye Cai[3], Wenji Li[2], Huibiao Lin[2], Zefeng Yu[2] and Jiewei Lu[2]

***Abstract*— Optic Disk (OD) detection plays an important role for fundus image analysis. In this paper, we propose an algorithm for detecting OD mainly based on a classifier model trained by structured learning. Then we use the model to achieve the edge map of OD. Thresholding is performed on the edge map to obtain a binary image. Finally, circle Hough transform is carried out to approximate the boundary of OD by a circle. The proposed algorithm has been evaluated on the public database and obtained promising results. The results (an area overlap and Dices coefficients of 0.8636 and 0.9196, respectively, an accuracy of 0.9770, and a true positive and false positive fraction of 0.9212 and 0.0106) show that the proposed method is a robust tool for the segmentation of OD and is very competitive with the stage-of-the-art methods.**

I. INTRODUCTION

Optic disk (OD) detection plays an important role in the fundus image analysis and computer aided diagnosis for ocular diseases, which has attracted extensive attentions from clinicians and researchers as an early stage detection method for ocular diseases. In addition, OD detection is often a key step for the detection of other anatomical structures [1], [2]. For example, the OD location helps to avoid false positive in the detection of exudates associated with diabetic retinopathy, since both of them are bright regions in the fundus image [3]. Besides, the vessels, which are of direct importance in assessing vascular condition, radiate from the OD, so tracking algorithms for vessels may start from there [2]. Moreover, the relationship between the size of the OD and the optic cup has been widely utilized for glaucoma diagnosis [3].

However, detecting OD automatically is not an easy job since the variations of the OD's shape, size, colour and so on. Many OD detection algorithms have been introduced in the literatures, which can mainly be classified as template based methods [4], [5], [6], deformable model based methods [2], [7], [8] and morphology based methods [3], [9], [10].

These methods have a common characteristic that is without using the mechanism of machine learning. With the rapid development of machine learning, the power of machine learning become more and more strong. But the research of using machine learning for OD detection is relative less. Far as we know, [11] is the only work using machine learning for OD detection and obtain very competitive results. In [11], the authors proposed an algorithm for OD detection based on super pixels classification. This method mainly utilizes the region information of the fundus image to detect the OD.

In this paper, we mainly utilize the edge information of the fundus image to detect the OD. It is different from the traditional method for OD detection using edge information. In the traditional approaches, the pre-processing, such as image enhancement, vessels elimination, is a key step to enhance the boundary of OD. Then edge detectors, such as Prewitt edge detector [12], are used to detect the OD edge.

However, the variety of the fundus image make the traditional edge detector difficult to meet the requirement. In addition, which channel of the original fundus image should be chosen as the input image is also difficult to decide due to the variability of the fundus image. Such as in [13], the green channel of the original RGB image is used. In [10], the red channel. Or even a combination of both of them [5]. However, due to the variability of the fundus image, they do not always provide the desired results [3].

Inspired by the method proposed by P. Dollár et al. [14] which used structured learning to detect the image edge, we proposed an algorithm for OD boundary detection which mainly based on structured learning. The input of the proposed method is the original fundus image thus there is no need to consider which form of the greyscale image of the original image should be chosen. In addition, there is no need for the algorithm to take extra steps to eliminate the blood vessels or enhance the image, since only the structure about OD boundary are fed to the learning algorithm.

The flowchart of the proposed method is shown in Fig.1. In training stage, we use the structured learning to obtain the model. Then we use the trained model to achieve the edge map of OD. Thresholding is performed on the edge map thus a binary image of OD is obtained. Finally, circle Hough transform is carried out to approximate the boundary of OD by a circle.

The proposed method has been evaluated on the MESSIDOR database [15] and the average values obtained (an area overlap and Dices coefficients of 0.8636 and 0.9196, respectively, an accuracy of 0.9770, and a true positive and false positive fraction of 0.9212 and 0.0106) show that the method is a robust tool for the segmentation of OD, and the experimental results also demonstrate that the proposed method is very competitive with the stage-of-the-art methods.

The rest of the paper is organized as follows: in Section II, the main stages of the proposed algorithm are described, mainly about OD edge detection using structured forests.

[1]Zhun Fan with Key Laboratory of Digital Signal and Image Processing of Guangdong Provincial, College of Engineering, Shantou University. 515063, Shantou, China. zfan@stu.edu.cn.

[2]Yibiao Rong, Wenji Li, Huibiao Lin, Zefeng Yu and Jiewei Lu with College of Engineering, Shantou University. 515063, Shantou, China. 13ybrong@stu.edu.cn, liwj@stu.edu.cn, 13hblin@stu.edu.cn, yuzf@stu.edu.cn, 12jwlu1@stu.edu.cn.

[3]Xinye Cai with school of computer science and technology, Nanjing University of Aeronautics and Astronautics, Jiangsu, China.xinye@nuaa.edu.cn.

978-1-4673-9674-5/15/$31.00 © 2015 IEEE

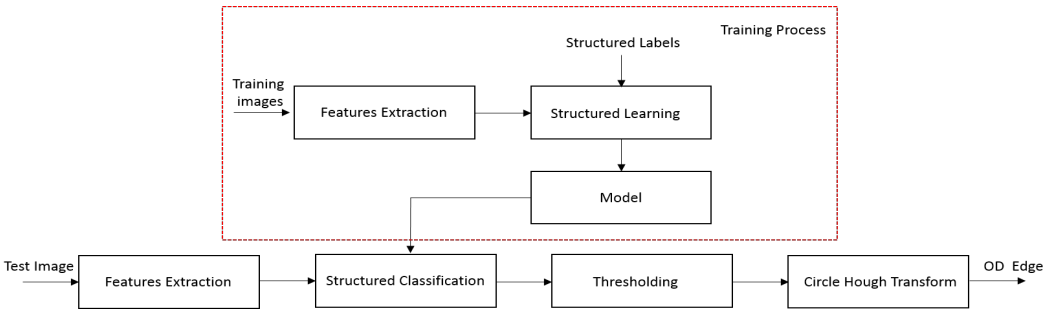

Fig. 1. The flow chart of the proposed algorithm.

Section III shows the experimental results obtained using the public database, and a comparison with other methods from the literatures. We provide discussion and conclusions in Section IV.

II. METHOD

A. Obtaining Edge Map by Structured Learning

Structured learning or structured prediction addresses the problem of learning a mapping where the input or output space may be arbitrarily complex representing strings, sequences, graphs, object pose, bounding boxes etc. [14], [16], [17]. Similar to commonly used supervised learning techniques, structured prediction function are typically trained by means of observed data in which the true prediction value is used to adjust model parameters. The prediction function is defined in such a way that the actual prediction $f(x)$ for a given instance $x \in X$ (input domain) is obtained by maximizing an auxiliary evaluation function $g : X \times Y \rightarrow R$ over all possible elements in Y (output domain), such that

$$y^* = f(x) = arg \max_{y \in Y} g(x, y) \tag{1}$$

To learn about the structured learning, we refer readers to [18] for a comprehensive survey.

Similar with general images, OD edge in a local patch of the fundus image are also highly interdependent [19]. They often contains well-known patterns, such as straight lines or arc. Since the output space of the structured learning can be arbitrarily complex representing, thus the problem of OD edge detection can be formulated as predicting local segmentation masks given input image patches. In this work, we take advantage of the method proposed by P. Dollár [14] where random forest is used to capture the structured information.

Random forest is an ensemble of T independent decision trees f_t, which consists of root node, split node and leaf node. Each split node stores a split function to be applied to the incoming data and each leaf node stores the final predictor. The split function is defined as:

$$h(x, \theta_j) \in \{0, 1\} \tag{2}$$

with parameters θ_j. If $h(x, \theta_j) = 1$, node j sends x right, otherwise left. The output of the tree on an input x is the prediction stored at the leaf node reached by x, which may be a target label $y \in Y$.

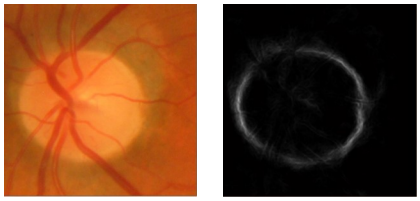

(a) (b)

Fig. 2. The schematic of structured learning based for OD edge map. (a) Fundus image, (b) Edge map .

Training decision tree is a process of optimizing parameters of the split functions associated with all the split nodes, as well as the leaf predictors. Split parameters θ_j are chosen when the information gain reaches maximum. The information gain is defined as:

$$I = H(S_j) - \sum_{k \in \{L,R\}} \frac{|S_j^k|}{|S_j|} H(S_j^k) \tag{3}$$

where $H(S) = -\sum_y p_y log(p_y)$ denotes the Shannon entropy and p_y is the fraction of elements in S with label y. $S_j^R = \{(x, y) \in S_j | h(x, \theta_j) = 1\}$ means the data are send to right, and $S_j^L = S_j \backslash S_j^R$ the data are send to left.

The main challenge of training random forest with structured labels is how to define the information gain. In [14], to learning decision trees uses structured labels to determine the splitting function at each branch in the tree, the structured labels are mapped to a discrete space on which standard information gain measures may be evaluated. Each tree predicts a patch of edge pixel labels that are aggregated across the image to compute the final edge map. The size of the input image patch is 32×32 . The features for each patch are extracted on a set of color and gradient channels [14], [20]. Fig.2 shows the schematic of the OD edge map obtained by structured learning, where Fig.2 (a) is a fundus image and Fig.2 (b) is the edge map of the fundus image.

B. Thresholding

Given a grayscale image , thresholding can be used to create a binary image. The threshloding methods replace each pixel in an image with a black pixel if the intensity $I(x, y)$ is less than some fixed value T, or a white pixel if the image intensity is greater than that value. This can be

(a) (b) (c)

Fig. 3. Different results when k is set to different values. (a) k is equal to 1, (b) k is equal to 0.618, (c) k is equal to 0.4

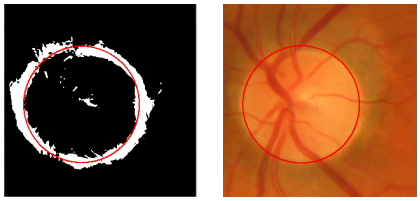

(a) (b)

Fig. 4. An example fit the OD boundary by circle. (a) Circular approximation of OD boundary. (b) Put the circle on the fundus image.

defined as:

$$BW(x,y) = \begin{cases} 1 & \text{if } I(x,y) > 0 \\ 0 & \text{others} \end{cases} \quad (4)$$

The key step of thresholding is to select the threshold T. In this work, we use Otsus method [21], which search for the threshold by minimizing the intra-class variance, to obtain the threshold. To protect more information of OD boudary, we reduce T by multiply a factor k which less than 1. Fig.3 shows the binary image when k is equal to 1, 0.618, 0.4, respectively. We can see that when k is smaller, more edge information are protected, at the same time, more false edge. In our work, we set k is equal to 0.618 by experiment.

C. Circle Hough Transform

The purpose of circle Hough transform is to find the circle patterns in the image [22]. The process of the Hough Transform is to transform a set of feature points in the image space into a set of accumulated votes in a parameter space. Then, for each feature point, votes are accumulated in an accumulator array for all parameter combinations. The array elements that contain the highest number of votes indicate the presence of the shape [23]. Based on the parametric equation of the circle, we can obtain the center and the radius of the circle by performing circle Hough transform on the image. It can be defined as [5]:

$$(c_x, c_y, r) = CHT(I_{BW}, r_{min}, r_{max}) \quad (5)$$

where I_{BW} is a binary image and (r_{min}, r_{max}) is the search range of the radius. (c_x, c_y) and r are respectively the center position and radius obtained by circle Hough transform.

According to the equation (5), the parameters of the circle Hough transform is the r_{min} and r_{max} . In this work, we set r_{min} is equal to 50 and r_{max} is equal to 90 according to the analysis of the [24], [5]. Fig.4 gives an example where the red circle is the approximation of the OD boundary detected by circle Hough transform.

III. RESULTS

The proposed algorithm has been evaluated on the public database MESSIDOR [15], which kindly provided by the Messidor program partners. It contains 1200 eye fundus color images. The images were acquired by 3 ophthalmologic departments using a color video 3CCD camera on a Topcon TRC NW6 non-mydriatic retinpgraph with 45 degree field of view. The images are 1440×960 , 2240×1488 or 2304×1536 pixels in size and 8 bits per color plane and are provided in TIFF format. 800 images were acquired with pupil dilation and 400 without dilation. The ground truth of these 1200 images is currently available online [25].

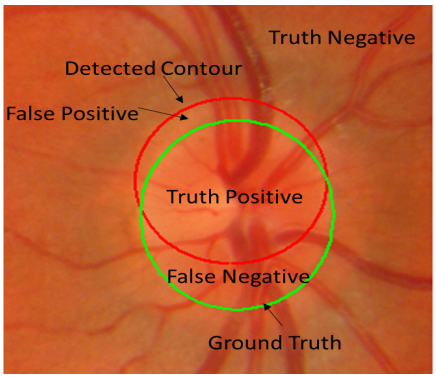

Fig. 5. The sketch map to illustrate the basic concepts of TP, FP, TN and FN.

The performance of the methods has been evaluated based on different concepts. We use the Fig.5 to illustrate the concepts. Let TP represents True Positive, FP False Positive, TN True Negative, and FN False Negative. Based on these basic concepts, Area Overlap (AOL), Dices (S) coefficients, Accuracy (Ac), True Positive Fraction (TPF) and False Positive Fraction (FPF) are defined as follow:

$$AOL = TP/(TP + FN + FP) \quad (6)$$

$$S = 2TP/(2TP + FN + FP) \quad (7)$$

$$Ac = (TP + TN)/(TP + TN + FP + FN) \quad (8)$$

$$TPF = TP/(TP + FN) \quad (9)$$

$$FPF = FP/(FP + FN) \quad (10)$$

In this work, we focus on the segmentation of OD, so a 300×300 sub-image, which include the region of interest, is extracted first. We use the method proposed by J. Lowell [2] to locate the OD. The accuracy of the locating is 97% in MESSIDOR database. For the images are not correctly to locate, we corrected them manually and used them to evaluate the performance of the algorithm for the segmentation of OD, too.

A. Parameters Evaluation

The proposed algorithm for segmentation of OD is mainly based on structured learning. The random forest is used to capture the structured information of the OD boundary. The

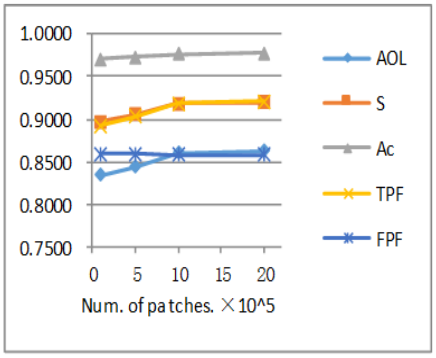

Fig. 6. The influence of the number of trained patches for the algorithm

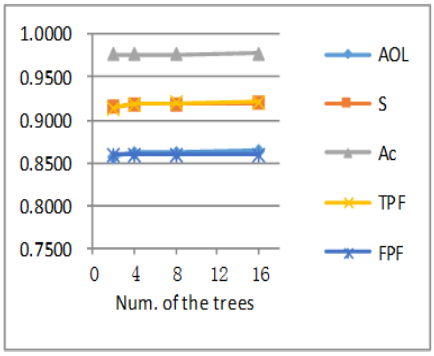

Fig. 7. The influence of the number of trees for the algorithm

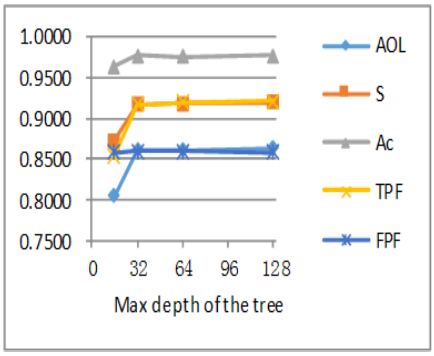

Fig. 8. The influence of the max depth of the tree for the algorithm

parameters that most influence the behavior of the decision forest are: the number of decision trees, the number of train patches and the max depth of the tree [26]. Since the proposed method is mainly based on supervised machine learning, K-fold cross validation [27] (We set K is equal to 12 since the images have been divided into 12 groups (each group contains 100 images) by the authors [15]) is used to evaluate the algorithm. We set default values for the parameters (the number of trained patches is 10^6, the number of trees is 8, the max depth of the tree is 64) then let one change and the others are equal to the default values, then explore the effect of the parameter. Since the FPF is smaller, to see the tendency clearly in the same figure, we map the FPF into the range of 0.75 to 1 equally. The map is defined as:

$$FPF' = \exp(FPF) \tag{11}$$

Fig.6 shows how varying the number of patches affects the results. It can be note that increasing the number of patches improves the results when the number is less than 10^6. After the number of trained patches is larger than 10^6, the performance of the algorithm tends to stabilize. In Fig.7, we plot the influence of the number of trees for the proposed algorithm. we can see that the proposed algorithm is not very sensitive to the number of trees. Increasing the number of trees improves the results slightly. Fig.8 shows how varying the max depth of the tree affects the results. It can be note that the performance of the algorithm is improving with the increase of the max depth of the tree when it is less than 32. After the max depth of the tree is greater than 32, the performance of the algorithm tends to be stable.

According to the analysis of Fig.6 to Fig.8, the number of train patches as 10^6, the number of trees as 8 and the max depth of the tree as 64 are good choices, neither too small to lose the precision nor too large to increase the burden on the computer. The average values obtained by the algorithm are: area overlap and Dices coefficients of 0.8636 and 0.9196, respectively, an accuracy of 0.9770, and a true positive and false positive fraction of 0.9212 and 0.0106.

Fig.9 shows some examples where red circles are the OD boundary detected by the proposed algorithm, and green circles are the ground truth. From these cases, we can see that when the detected boundary are included in the ground truth, such as (d), an ideal value of FPF is achieved even though the result is not perfect actually. When the ground truth are included in the detected boundary, such as (c), an ideal value of TPF is obtained even though the result is not perfect, either. So, the indicators TPF and FPF just can only evaluate the performance of the algorithm one-sided. In addition, the AOL is more sensitive to the results than Ac. This can be illustrated by comparing (a) and (b), where AOL=0.9815, Ac=0.9938 in (a) and AOL=0.8540, Ac=0.9911 in (b). It means that for a deteriorating result the AOL has more obviously change. It also can be illustrated in case of (e) when a bad result is obtained, the AOL is obviously worse than the Ac.

B. Comparison with Other Algorithms

In this work, we select the methods proposed by S. Morales et al.[3] and A. Aquino et al. [5], which are considered as the state-of-the-art methods for OD detection, to compare.

Table I shows the results comparison with S. Morales' method. It can be note that the AOL and S obtained by the proposed method are improved comparing with the method proposed by S. Morales. For the Ac, TPF, FPF, the results obtained by the proposed method is not as good as those of the S. Morales. But as we illustrate before, the Ac is less sensitive to the results, and the TPF, FPF just can evaluate the performance of the algorithm one-sided. From this point

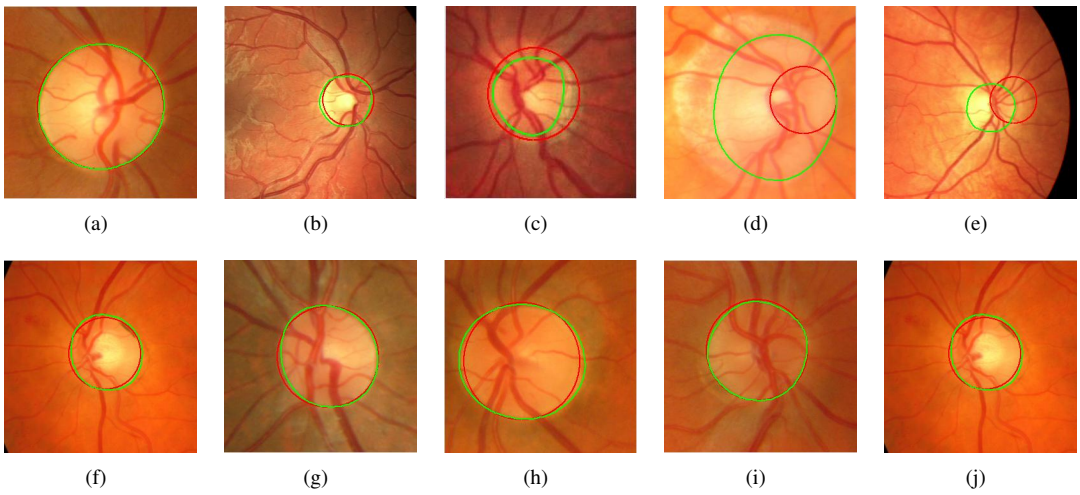

Fig. 9. Some examples where green circles are the ground truth and red circles are the circle detected by the proposed algorithm. (a). AOL=0.9815, S=0.9907, Ac=0.9938, TPF=0.9946, FPF=0.0066. (b). AOL=0.8540, S=0.9213, Ac=0.9911, TPF=0.9723, FPF=0.0037. (c). AOL=0.6678, S=0.8008, Ac=0.9399, TPF=1, FPF=0.0683. (d). AOL=0.2478, S=0.3971, Ac=0.7154, TPF=0.2478, FPF=0. (e). AOL=0.2358, S=0.3816, Ac=0.9414, TPF=0.0362, FPF=0.0283. (f). AOL=0.8983, S=0.9464, Ac=0.9880, TPF=0.9200, FPF=0.003. (g). AOL=0.9339, S=0.9658, Ac=0.9854, TPF=0.9820, FPF=0.0137. (h). AOL=0.9173, S=0.9569, Ac=0.9743, TPF=0.9260, FPF=0.0042. (i). AOL=0.9513, S=0.9751, Ac=0.9894, TPF=0.9976, FPF=0.0127. (j). AOL=0.8983, S=0.9464, Ac=0.9880, TPF=0.9200, FPF=0.0031.

of view, the performance of the proposed algorithm may be better.

TABLE I
COMPARISON OF THE METRICS (AVERAGE VALUES AND STANDARD DEVIATIONS) OF OBTAINED BY THE PROPOSED METHOD, BY THE PCA AND MATHEMATICAL MORPHOLOGY BASED METHOD

	Proposed	S. Morales [3]
AOL	0.8636(0.1268)	0.8228(0.1384)
S	0.9196(0.1019)	0.8950(0.1056)
Ac	0.9770(0.0284)	0.9949(0.0050)
TPF	0.9212(0.1213)	0.9300(0.1239)
FPF	0.0106(0.0129)	0.0035(0.0041)

Table II shows the results compare with the method proposed by A. Aquino [5]. Data are presented in columns as the percentage of images per interval of area overlap values, the last column is the total average of the area overlap values. The first five rows of the Table II summarizes the performance of the template based method proposed by A. Aquino [5]. The first row shows the results for the elliptical approach based on minimizing the geometric distance, the following three rows shows the results obtained with three variants based on minimizing the algebraic distance, and the fifth row shows the results of the circular approach. It can be seen that the elliptical approach is significantly poorer, three of the elliptical template-based variants were based on minimizing the algebraic distance achieving an $\overline{AOL} \approx 0.66$, and the one based on minimizing the geometric distance achieving an $\overline{AOL} \approx 0.67$. The proposed method improves the performance of all elliptical approaches and achieves comparable results with the circular template-based method ($\overline{AOL} = 0.86$).

IV. DISCUSSION AND CONCLUSION

In this paper, a new algorithm for the automatic detection of OD has been presented. The proposed algorithm mainly consists of three steps: obtaining the edge map based on structured forests, performing the thresholding on the edge map and approximating the OD boundary by a circle.

Compare with the methods which also mainly use the edge information to detect the OD, the proposed algorithm use the structured forests to capture the information and the process of the proposed algorithm is simpler since pre-processing, such as image enhancement, vessels elimination, are no need. Moreover, the input of the proposed algorithm is the original image so there is no need to consider which channel of the image as the input which usually is difficult to decide for many algorithms of OD detection due to the variability of the fundus image.

Once we obtained the trained model, the average computational time obtained for OD segmentation is 1.7494s with a standard deviation of 0.2987s performed on a PC equipped with an Intel (R) Core (TM) i-5 4210 M CPU at 2.60 GHZ and 4 GB of RAM capacity using MATLAB and the results are very competitive with the state-of-the-art methods.

The main disadvantage of the proposed method is that the boundary of the OD is approximated by a circle. Although promising results are achieved, the true OD boundary is hard to obtain. To improve the performance of the proposed algorithm, the circle obtained by the proposed algorithm may be used as the initial contour for a deformable model. But how to design a robust force according to the characteristic of the fundus image is our future work.

ACKNOWLEDGMENT

This research work was supported by Guangdong Key Laboratory of Digital Signal and Image Processing, the National Natural Science Foundation of China

TABLE II
COMPARISON BETWEEN THE PROPOSED METHOD AND ONE CIRCULAR TEMPLATE-BASED METHOD AND FOUR ELLIPTICAL TEMPLATE-BASED METHODS. DATA IN TERMS OF PERCENTAGE OF IMAGES PER AREA OVERLAP INTERVAL AND AVERAGE AREA OVERLAP OF THE WHOLE MESSIDOR DATABASE

	$AOL \geq 0.95$	$AOL \geq 0.90$	$AOL \geq 0.85$	$AOL \geq 0.80$	$AOL \geq 0.70$	$\overline{AOL}$
Elliptical Geometrical Min.[5]	2%	11%	20%	30%	51%	0.6700
Elliptical Algebraic Min1.[5]	2%	9%	17%	26%	48%	0.6600
Elliptical Algebraic Min2.[5]	2%	10%	19%	27%	47%	0.6500
Elliptical Algebraic Min3.[5]	2%	9%	18%	26%	48%	0.6600
Circular Hough.[5]	7%	46%	73%	84%	93%	0.8600
Proposed	7%	51%	78%	86%	93%	0.8636

under Grant (61175073, 61300159, 61332002, 51375287, 61370102, 61170193), Jiangsu Natural Science Foundation (BK20130808).Innovative Application and Integrated Services Platform of the First Generation of Numerical Control in the Eastern Part of Guangdong Province, support no. (2013B011304002).

REFERENCES

[1] S. Lu, "Accurate and efficient optic disc detection and segmentation by a circular transformation," *Medical Imaging, IEEE Transactions on*, vol. 30, no. 12, pp. 2126–2133, 2011.

[2] J. Lowell, A. Hunter, D. Steel, A. Basu, R. Ryder, E. Fletcher, and L. Kennedy, "Optic nerve head segmentation," *Medical Imaging, IEEE Transactions on*, vol. 23, no. 2, pp. 256–264, 2004.

[3] S. Morales, V. Naranjo, J. Angulo, and M. Alcañiz, "Automatic detection of optic disc based on pca and mathematical morphology," *Medical Imaging, IEEE Transactions on*, vol. 32, no. 4, pp. 786–796, 2013.

[4] M. Park, J. S. Jin, and S. Luo, "Locating the optic disc in retinal images," in *Computer Graphics, Imaging and Visualisation, 2006 International Conference on*. IEEE, 2006, pp. 141–145.

[5] A. Aquino, M. E. Gegúndez-Arias, and D. Marín, "Detecting the optic disc boundary in digital fundus images using morphological, edge detection, and feature extraction techniques," *Medical Imaging, IEEE Transactions on*, vol. 29, no. 11, pp. 1860–1869, 2010.

[6] M. Lalonde, M. Beaulieu, and L. Gagnon, "Fast and robust optic disc detection using pyramidal decomposition and hausdorff-based template matching," *Medical Imaging, IEEE Transactions on*, vol. 20, no. 11, pp. 1193–1200, 2001.

[7] A. Osareh, M. Mirmehdi, B. Thomas, and R. Markham, "Comparison of colour spaces for optic disc localisation in retinal images," in *Pattern Recognition, 2002. Proceedings. 16th International Conference on*, vol. 1. IEEE, 2002, pp. 743–746.

[8] H. Li and O. Chutatape, "Automated feature extraction in color retinal images by a model based approach," *Biomedical Engineering, IEEE Transactions on*, vol. 51, no. 2, pp. 246–254, 2004.

[9] T. Walter, J.-C. Klein, P. Massin, and A. Erginay, "A contribution of image processing to the diagnosis of diabetic retinopathy-detection of exudates in color fundus images of the human retina," *Medical Imaging, IEEE Transactions on*, vol. 21, no. 10, pp. 1236–1243, 2002.

[10] D. Welfer, J. Scharcanski, C. M. Kitamura, M. M. Dal Pizzol, L. W. Ludwig, and D. R. Marinho, "Segmentation of the optic disk in color eye fundus images using an adaptive morphological approach," *Computers in Biology and Medicine*, vol. 40, no. 2, pp. 124–137, 2010.

[11] J. Cheng, J. Liu, Y. Xu, F. Yin, D. W. K. Wong, N.-M. Tan, D. Tao, C.-Y. Cheng, T. Aung, and T. Y. Wong, "Superpixel classification based optic disc and optic cup segmentation for glaucoma screening," *Medical Imaging, IEEE Transactions on*, vol. 32, no. 6, pp. 1019–1032, 2013.

[12] R. C. Gonzalez, *Digital image processing*. Pearson Education India, 2009.

[13] M. Niemeijer, M. D. Abràmoff, and B. Van Ginneken, "Fast detection of the optic disc and fovea in color fundus photographs," *Medical image analysis*, vol. 13, no. 6, pp. 859–870, 2009.

[14] P. Dollár and C. L. Zitnick, "Fast edge detection using structured forests," 2014.

[15] M. T.-V. Project, "Messidor: Digital retinal images france," 2008. [Online]. Available: [Online].Available: http://messidor.crihan.fr/download-en.php

[16] B. Taskar, V. Chatalbashev, D. Koller, and C. Guestrin, "Learning structured prediction models: A large margin approach," in *Proceedings of the 22nd international conference on Machine learning*. ACM, 2005, pp. 896–903.

[17] M. B. Blaschko and C. H. Lampert, "Learning to localize objects with structured output regression," in *Computer Vision–ECCV 2008*. Springer, 2008, pp. 2–15.

[18] S. Nowozin and C. H. Lampert, "Structured learning and prediction in computer vision," *Foundations and Trends® in Computer Graphics and Vision*, vol. 6, no. 3–4, pp. 185–365, 2011.

[19] J. J. Lim, C. L. Zitnick, and P. Dollár, "Sketch tokens: A learned mid-level representation for contour and object detection," in *Computer Vision and Pattern Recognition (CVPR), 2013 IEEE Conference on*. IEEE, 2013, pp. 3158–3165.

[20] P. Dollár, Z. Tu, P. Perona, and S. Belongie, "Integral channel features." in *BMVC*, vol. 2, no. 3, 2009, p. 5.

[21] N. Otsu, "A threshold selection method from gray-level histograms," *Automatica*, vol. 11, no. 285-296, pp. 23–27, 1975.

[22] J. Illingworth and J. Kittle, "The adaptive hough transform," *Pattern Analysis and Machine Intelligence, IEEE Transactions on*, no. 5, pp. 690–698, 1987.

[23] H. P. VC, "Method and means for recognizing complex patterns," Dec. 18 1962, uS Patent 3,069,654.

[24] H. Li and O. Chutatape, "Automatic location of optic disk in retinal images," in *Image Processing, 2001. Proceedings. 2001 International Conference on*, vol. 2. IEEE, 2001, pp. 837–840.

[25] U. Huelva, "Expert system for early automated detection of od by analysis of digital retinal images project website," Sep. 24,2012. [Online]. Available: [Online]. Available: http://www.uhu.es/retinopathy/muestras.php

[26] A. Criminisi, J. Shotton, and E. Konukoglu, *Decision forests: A unified framework for classification, regression, density estimation, manifold learning and semi-supervised learning*. Now, 2012.

[27] S. Rogers and M. Girolami, *A first course in machine learning*. CRC Press, 2011.